Imaging with second-harmonic radiation probes in living tissue

Rachel Grange,[1,2,*] Thomas Lanvin,[1] Chia-Lung Hsieh,[1,3] Ye Pu,[1] and Demetri Psaltis[1]

[1]*Laboratory of Optics, School of Engineering, EPFL, Station 17, 1015 Lausanne, Switzerland*
[2]*Multiphoton Laboratory, Institute of Applied Physics, Friedrich Schiller University, Albert-Einstein-Str. 15, 07745 Jena, Germany*
[3]*Department of Electrical Engineering, California Institute of Technology, 1200 East California Boulevard, MC 136-93, Pasadena, California 91125, USA*
rachel.grange@uni-jena.de

Abstract: We demonstrate that second-harmonic radiation imaging probes are efficient biomarkers for imaging in living tissue. We show that 100 nm and 300 nm $BaTiO_3$ nanoparticles used as contrast markers could be detected through 50 μm and 120 μm of mouse tail tissue in vitro or in vivo. Experimental results and Monte-Carlo simulations are in good agreement.

OCIS codes: (110.0113) Imaging through turbid media; (160.4236) Nanomaterials; (160.4330) Nonlinear optical materials; (180.5810) Scanning microscopy; (290.7050) Turbid media

References and links

1. I. M. Vellekoop and A. P. Mosk, "Focusing coherent light through opaque strongly scattering media," Opt. Lett. **32**(16), 2309–2311 (2007).
2. E. Gratton, "Applied physics. Deeper tissue imaging with total detection," Science **331**(6020), 1016–1017 (2011).
3. C.-L. Hsieh, Y. Pu, R. Grange, G. Laporte, and D. Psaltis, "Imaging through turbid layers by scanning the phase conjugated second harmonic radiation from a nanoparticle," Opt. Express **18**(20), 20723–20731 (2010).
4. W. Denk, J. H. Strickler, and W. W. Webb, "Two-photon laser scanning fluorescence microscopy," Science **248**(4951), 73–76 (1990).
5. F. Helmchen and W. Denk, "Deep tissue two-photon microscopy," Nat. Methods **2**(12), 932–940 (2005).
6. B. N. G. Giepmans, S. R. Adams, M. H. Ellisman, and R. Y. Tsien, "The fluorescent toolbox for assessing protein location and function," Science **312**(5771), 217–224 (2006).
7. R. M. Dickson, A. B. Cubitt, R. Y. Tsien, and W. E. Moerner, "On/off blinking and switching behaviour of single molecules of green fluorescent protein," Nature **388**(6640), 355–358 (1997).
8. L. L. Xuan, S. Brasselet, F. Treussart, J. F. Roch, F. Marquier, D. Chauvat, S. Perruchas, C. Tard, and T. Gacoin, "Balanced homodyne detection of second-harmonic generation from isolated subwavelength emitters," Appl. Phys. Lett. **89**(12), 121118 (2006).
9. L. Bonacina, Y. Mugnier, F. Courvoisier, R. Le Dantec, J. Extermann, Y. Lambert, V. Boutou, C. Galez, and J. P. Wolf, "Polar Fe(IO3)(3) nanocrystals as local probes for nonlinear microscopy," Appl. Phys. B **87**(3), 399–403 (2007).
10. A. V. Kachynski, A. N. Kuzmin, M. Nyk, I. Roy, and P. N. Prasad, "Zinc oxide nanocrystals for nonresonant nonlinear optical microscopy in biology and medicine," J. Phys. Chem. C **112**(29), 10721–10724 (2008).
11. Y. Pu, M. Centurion, and D. Psaltis, "Harmonic holography: a new holographic principle," Appl. Opt. **47**(4), A103–A110 (2008).
12. E. Delahaye, N. Tancrez, T. Yi, I. Ledoux, J. Zyss, S. Brasselet, and R. Clement, "Second harmonic generation from individual hybrid $MnPS_3$-based nanoparticles investigated by nonlinear microscopy," Chem. Phys. Lett. **429**(4-6), 533–537 (2006).
13. C.-L. Hsieh, R. Grange, Y. Pu, and D. Psaltis, "Three-dimensional harmonic holographic microcopy using nanoparticles as probes for cell imaging," Opt. Express **17**(4), 2880–2891 (2009).
14. C.-L. Hsieh, R. Grange, Y. Pu, and D. Psaltis, "Characterization of the cytotoxicity and imaging properties of second-harmonic nanoparticles," Proc. SPIE **7759**, 77590T, 77590T-6 (2010).
15. G. Ciofani, S. Danti, S. Moscato, L. Albertazzi, D. D'Alessandro, D. Dinucci, F. Chiellini, M. Petrini, and A. Menciassi, "Preparation of stable dispersion of barium titanate nanoparticles: Potential applications in biomedicine," Colloids Surf. B Biointerfaces **76**(2), 535–543 (2010).
16. Y. Pu, R. Grange, C.-L. Hsieh, and D. Psaltis, "Nonlinear optical properties of core-shell nanocavities for enhanced second-harmonic generation," Phys. Rev. Lett. **104**(20), 207402 (2010).

#149795 - $15.00 USD Received 24 Jun 2011; revised 29 Jul 2011; accepted 29 Jul 2011; published 2 Aug 2011

17. C.-L. Hsieh, R. Grange, Y. Pu, and D. Psaltis, "Bioconjugation of barium titanate nanocrystals with immunoglobulin G antibody for second harmonic radiation imaging probes," Biomaterials **31**(8), 2272–2277 (2010).
18. J. Extermann, L. Bonacina, E. Cuña, C. Kasparian, Y. Mugnier, T. Feurer, and J.-P. Wolf, "Nanodoublers as deep imaging markers for multi-photon microscopy," Opt. Express **17**(17), 15342–15349 (2009).
19. P. Pantazis, J. Maloney, D. Wu, and S. E. Fraser, "Second harmonic generating (SHG) nanoprobes for in vivo imaging," Proc. Natl. Acad. Sci. U.S.A. **107**(33), 14535–14540 (2010).
20. P. J. Campagnola and L. M. Loew, "Second-harmonic imaging microscopy for visualizing biomolecular arrays in cells, tissues and organisms," Nat. Biotechnol. **21**(11), 1356–1360 (2003).
21. M. T. Buscaglia, V. Buscaglia, and R. Alessio, "Coating of $BaCO_3$ Crystals with TiO_2:Versatile Approach to the Synthesis of $BaTiO_3$ Tetragonal Nanoparticles," Chem. Mater. **19**(4), 711–718 (2007).
22. K. König, P. T. C. So, W. W. Mantulin, and E. Gratton, "Cellular response to near-infrared femtosecond laser pulses in two-photon microscopes," Opt. Lett. **22**(2), 135–136 (1997).
23. P. Stoller, B.-M. Kim, A. M. Rubenchik, K. M. Reiser, and L. B. Da Silva, "Polarization-dependent optical second-harmonic imaging of a rat-tail tendon," J. Biomed. Opt. **7**(2), 205–214 (2002).
24. C.-L. Hsieh, Y. Pu, R. Grange, and D. Psaltis, "Second harmonic generation from nanocrystals under linearly and circularly polarized excitations," Opt. Express **18**(11), 11917–11932 (2010).
25. L. Wang, S. L. Jacques, and L. Zheng, "MCML—Monte Carlo modeling of light transport in multi-layered tissues," Comput. Methods Programs Biomed. **47**(2), 131–146 (1995).
26. W. F. Cheong, S. A. Prahl, and A. J. Welch, "A review of the optical-properties of biological tissues," IEEE J. Quantum Electron. **26**(12), 2166–2185 (1990).
27. B. B. Das, F. Liu, and R. R. Alfano, "Time-resolved fluorescence and photon migration studies in biomedical and model random media," Rep. Prog. Phys. **60**(2), 227–292 (1997).

1. Introduction

Optical microscopy has been one of the most important tools in biology for almost a century. Images with ever higher resolution or contrast have been achieved over the years either by improving the optical techniques or using markers, such as green fluorescent proteins (GFPs) or quantum dots (QDs). Despite recent advances in the field of imaging through turbid media [1–3], it remains a challenge to optically penetrate tissues and perform in vivo imaging without surgery. Multiphoton microscopy improved the penetration depth by using pulsed near infrared laser light thereby decreasing the scattering and the excitation volume [4,5]. Multiphoton microscopy often relies on the use of fluorescent markers such as GFPs and QDs to specifically enhance the contrast of selected targets [6]. Those fluorophores are small and sensitive but are often limited by photobleaching, emission blinking, and phototoxicity [7].

Recently, a novel class of optical imaging markers have been introduced [8–12], which emit light through the second-harmonic generation (SHG) mechanism rather than the widely used fluorescence. SHG is a nonlinear quadratic process only present in a non-centrosymmetric environment. For example materials with non-centrosymmetric crystal structure generally produce SHG. We refer to this class of biomarkers as Second Harmonic Radiation IMaging Probes (SHRIMPs). SHRIMPs possess several key features, including long-term observation without photobleaching, flexibility in the choice of the excitation wavelength, coherent signals for scanningless 3D imaging [11,13], narrow signal bandwidth for greater noise rejection, ultrafast response time, and excellent biocompatibility [14,15]. These properties offer new modalities that are of interest in cell tracking experiments over long period of time, such as embryo development, or in 3D localization using interferometric detection. Moreover the recent demonstration of enhancement of the SHG signal with core-shell SHRIMPs provides high brightness for optimal contrast [16].

The SHG properties of several kinds of nanocrystals have been recently reported: KTP [8], $Fe(IO_3)_3$ [9], ZnO [10], $BaTiO_3$ [11] and organic/inorganic hybrid nanocrystals [12]. Specific labeling of SHG nanocrystals to biological target molecules has been developed with ZnO and $BaTiO_3$ nanoparticles [10,17]. Later on, more specific properties of the SHRIMPs were used such as the coherence of the emitted radiation by imaging through turbid media via digital phase conjugation [3]. SHRIMPs have been demonstrated as efficient biomarkers under 20 μm of in vitro liver tissue [18], and used in vivo in optically transparent zebra fish [19].

#149795 - $15.00 USD Received 24 Jun 2011; revised 29 Jul 2011; accepted 29 Jul 2011; published 2 Aug 2011

In this paper, we study for the first time the efficiency of 100 nm and 300 nm $BaTiO_3$ SHRIMPs in nontransparent tissues. We use in vitro tissues and in vivo tails of rodents. We show that the nanoparticles are clearly detectable even in the presence of strong endogenous SHG from collagen [20], and tissue scattering. We model the experiments with a Monte Carlo simulation to interpret our results.

2. Experimental results

The in vitro measurements were taken in the simple apparatus shown in Fig. 1 (a). The excitation light source is a linearly polarized femtosecond laser (Coherent Chameleon Ultra) at a center wavelength of 812 nm. A commercial scanning confocal microscope (Leica, SP5, DM6000) is used to image the samples. The laser was focused by a long working-distance 20x water immersion microscope objective with a large numerical aperture of 1.0. The reflected signal is sent through a band pass (350-680 nm band width) filter filtering out the near infrared light. The SHG signal and the fluorescence are collected in an epi-geometry simultaneously through two independent photomultipliers (PMT) via a dichroic filter with a cutting edge at 470 nm. The transmission through the dichroic filter is collected as the fluorescence signal. In the reflected SHG channel, a filter centered at 406 nm with a 15 nm bandwidth is used. The images are taken with a four times frame averaging for best quality. The pixel dwell time is on the order of microseconds and the incident pulse is not precompensated.

We choose $BaTiO_3$ nanoparticles because of the high second-order susceptibility tensor, which makes them a good marker for second-harmonic imaging. Moreover, this material is easily available, and its excellent biocompatibility was recently demonstrated [14,15]. The 100 nm particles have been characterized by dynamic light scattering [13]. The 300 nm $BaTiO_3$ nanoparticles were measured by a scanning electron microscope giving an average diameter measurements over 1000 nanoparticles of 280 nm [21]. For the in-vitro experiments, the particles in powder form were suspended in methanol and dispersed on a microscope glass slide. Prior each use, the solution was ultrasonicated to obtain a uniform suspension. For the in vivo experiments, the particles were suspended in deionized water and ultrasonicated before taking a small amount for the injection. No surface coating was used in the present study as compared with previous works in cells [13,17].

The in vitro sample preparation consists of depositing a droplet of the $BaTiO_3$ SHRIMPs (concentration 6 mg/4 ml) diluted in methanol on a glass slide and adding a controlled thickness of mouse tail (20 to 200 μm thick) tissue on top via conventional histology preparation (Fig. 1 (a)). The samples are conserved in phosphate buffered saline (PBS) solution with a cover glass. The laser light is focused through a water immersion lens on the nanoparticles under the mouse tail tissue and the cover glass. The peak intensity at the sample position is 13.2 GW/cm^2 nearly 10 times smaller than the cell damage threshold of 100 GW/cm^2 [22]. Figure 1 (b) shows the cross section image of the sample where the 300 nm SHRIMPs are readily detectable under 120 μm of mouse tail tissue in the presence of a strong endogenous SHG from the top layer of the sample. The endogenous SHG mainly comes from the dermal collagen present at the upper part of the tissue close to the air interface, which is followed by tissues without endogenous SHG and the SHRIMPs layer on the glass slide [23]. In Fig. 1 (b), the SHRIMPs are shown as elongated bright spots due to the scattering of the turbid medium, the lower axial resolution of the microscope and the aberration caused by the interface between the tissue and the immersion water. Moreover, some SHRIMPs were displaced from the glass slide and did not lie on a single plane as they were before the histology procedure. This is because during the sample preparation some of the SHRIMPs did not stick to the glass due to the pressure applied while positioning the layer of the tissue.

#149795 - $15.00 USD Received 24 Jun 2011; revised 29 Jul 2011; accepted 29 Jul 2011; published 2 Aug 2011

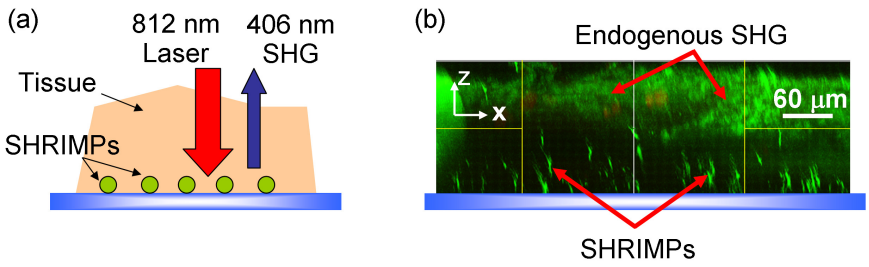

Fig. 1. In vitro sample for SHG imaging. (a) Sample diagram (b) Scanning confocal imaging of 300 nm SHRIMPs embedded 120 µm below an in vitro mouse tail tissue. (The pixel sizes are x and y = 1.52 µm, z = 168 nm).

Figure 2 (a-c) show section (x-y plane) images of 300 nm SHRIMPs with no tissue, 20 µm and 120 µm of mouse tail tissue on top of the SHRIMPs. By showing the SHG signal of isolated SHRIMPs, we can better see the effect of the different tissue thicknesses. On these images (Fig. 2 (a-c)), we observe the increase of the background noise with increasing tissue thicknesses. It is worth mentioning that the incident 812 nm light and the measured 406 nm light are scattered differently. This wavelength dependent effect can explain the not so strong alteration of the point spread function at 406 nm on Fig. 2 (a-c).

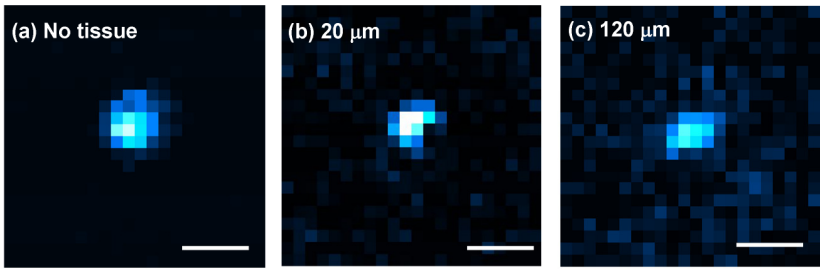

Fig. 2. SHG confocal section images (x-y plane) of 300 nm SHRIMPs with (a) no tissue, (b) 20 µm (c) 120 µm of in vitro tissue. Scale bar of 2 µm.

To quantify the results of the contrast of the SHRIMPs for different thicknesses of the in vitro tissue, we calculated an averaged signal-to-noise ratio (SNR) of several SHRIMPs in the corresponding section (x-y plane) images. The signal of a SHRIMP is calculated as the average intensity within the bright spot. This averaging of the intensity is needed because the signal of each nanoparticle will vary with the incident laser polarization according to its orientation. Indeed, the SHG signal is polarization and orientation sensitive since SHG is a coherent process [24].The noise is defined as the standard deviation of the fluctuating background. We expect two main sources of noise: the endogenous SHG and the detector noise. For SHG scanning microscopes, the signal mostly takes place at the focal point of the objective due to the optical nonlinearity and therefore, optical sectioning can be achieved [20]. However, when imaging with a sample with significant endogenous SHG at the surface, we noticed that the out-of-focus endogenous SHG sources contribute as additional noise in the image which is considerable compared to the detector noise.

The average SNR for different thicknesses of the tissue are plotted in Fig. 3. We observe the decay of the averaged SNR that is spanning from 366 for SHRIMPs with no tissue to 9 for SHRIMPs below 120 µm of mouse tail tissue (Fig. 3). The error bars are the standard deviation from up to 60 isolated SHRIMPs SNR measurements. The decrease in SNR is mostly due to the decrease of SHG signal; when the SHRIMP is deep in the scattering tissue, the excitation is scattered before reaching the SHRIMP, and the SHG signal generated from the SHRIMP is also being scattered before being collected by the microscope objective. We

#149795 - $15.00 USD Received 24 Jun 2011; revised 29 Jul 2011; accepted 29 Jul 2011; published 2 Aug 2011

will discuss the single exponential decay in SHG signal as a function of tissue thickness later in the text where we use a Monte Carlo simulation to estimate the effect.

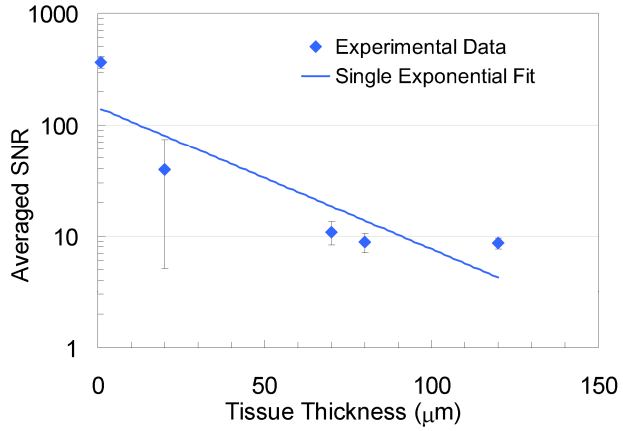

Fig. 3. Lin-log plot of the averaged signal-to-noise ratio from several 300 nm SHRIMPs located under in vitro tissue of different thicknesses.

Similarly, we prepared in vitro sample with $BaTiO_3$ SHRIMPs of 100 nm in diameter under 50, 80, 100 μm of mouse tail tissue. We detected few SHRIMPs under 50 μm of tissue as shown on Fig. 4 (a), and not under thicker tissue. We calculated a SNR of 8 for this limited numbers of SHRIMP. For comparison in Fig. 4 (b), we display the 300 nm SHRIMPs under 120 um of tissue, which has a SNR of 9.

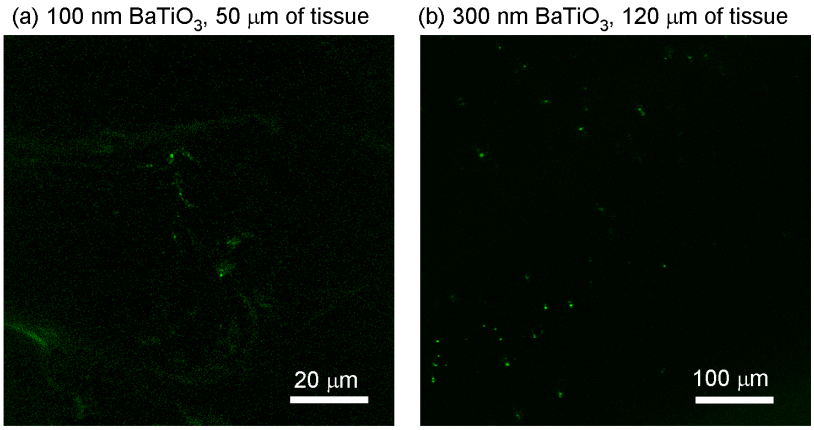

Fig. 4. SHG confocal section images (x-y plane) of (a) 100 nm SHRIMPs under 50 μm of in vitro tissue (the pixel sizes are x and y = 138 nm) and (b) 300 nm SHRIMPs under 120 um of tissue (the pixel sizes are x and y = 168 nm).

For the in vivo experiments, we first anesthetize the mouse by an intraperitoneal injection of xylasine/ketamine. We then used a syringe with a 350 μm needle to inject the 300 nm nanoparticles ($2 \cdot 10^{10}$ particles/ml) in distilled water (5 to 10 μl) around the middle of the tail of the living mouse. We bent the needle to inject the particles just under the skin and not in the blood flow. The injection site was marked with a pen for the convenience of relocation under the microscope. The mouse is then placed under the microscope objective with the tail immersed in water for matching the objective requirement (Fig. 5 (a)). After two hours of imaging experiments and before the animal woke up, the animal was sacrificed by cervical dislocation.

#149795 - $15.00 USD Received 24 Jun 2011; revised 29 Jul 2011; accepted 29 Jul 2011; published 2 Aug 2011

We can observe second harmonic signals from nanoparticles as deep as 100 μm below the surface of the tail with a SNR of 9 (Fig. 5 (b)). As with the in vitro experiment, a z-scan allows for imaging a superposition of section x-y planes of the mouse tail. The (x-z) section view of Fig. 5 (b) shows the elongated point spread function (PSF) of the SHRIMP due, again, to the scattering of the turbid medium the axial resolution of the microscope, and some aberration. Note that we look at the particles from the injections sites and track their positions under the skin tail. Few millimeters away from the injection site, no particles-like SHG signal was observed. This reasonably confirms that the signal we obtained was from SHRIMP rather than collagen aggregates.

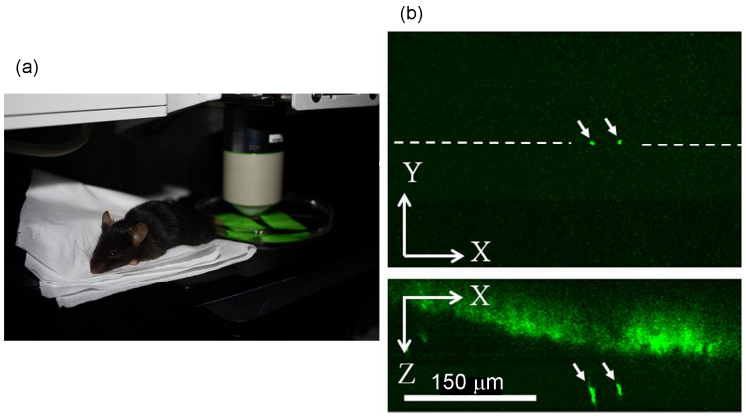

Fig. 5. In vivo sample for SHG imaging. (a) Sample diagram (b) Scanning confocal imaging of SHRIMPs embedded 100 μm below a mouse tail tissue. (The pixel sizes are x and y = 379 nm, z = 881 nm). The arrows show the same SHRIMPs on both views.

Both in vitro and in vivo experiments allow imaging the SHRIMPs as deep as 100 μm with sufficient contrast to distinguish them from endogenous second-harmonic from the tissue itself. The experimental results show that the endogenous SHG situated above the nanoparticles but contributing to the background noise still allow distinguishing the 300 nm nanoparticles located deeper in the tissue. It is worth mentioning that the power used in this experiment is close to 10 times smaller than the cell damage threshold and might be increased to see deeper in the tissue without risk of damage. This first in vivo trial was performed with 300 nm nanoparticles, a relative large size. However, we will be able to reduce the size of the nanoparticles either by increasing the intensity or by using core-shell nanocavities that can strongly enhance the SHG signal [16]. Moreover, we used an excitation wavelength very near in the infrared (812 nm); by increasing it further towards the infrared, the scattering will decrease and deeper imaging can then be possible [18].

3. Monte Carlo simulation

We carried out a Monte Carlo simulation to estimate the detected SHG signal of the SHRIMP at different depths of the scattering tissue [25]. This stochastic method provides a good estimate of the light behavior in highly absorbing and scattering media and it has been successfully applied to SHG from nanoparticles [18]. The model consists of two successive Monte Carlo simulations connected with a wavelength conversion by a single SHRIMP. The first simulation estimates the excitation light that reaches the SHRIMP through a certain tissue thickness and the second one estimates the SHG signal being detected after passing again through the tissue. The first run of the simulation used input parameters related to the 812 nm incident laser light, while the second run used the SHG light at 406 nm. The efficiency of the wavelength conversion of a single SHRIMP is modeled by the SHG cross-section using a previous model [16].

#149795 - $15.00 USD Received 24 Jun 2011; revised 29 Jul 2011; accepted 29 Jul 2011; published 2 Aug 2011

The method simulates the behavior of a very large number of photon ($3 \cdot 10^6$ photons), having a certain probability to be absorbed or scattered by the media cut in many successive layers from the input to the output surface. In our case, we divide the layer in 500 x 500 array of elements with a depth $dz = 2 \cdot 10^{-6}$ cm and width $dr = 2 \cdot 10^{-6}$ cm. The tissue parameters for the excitation and SHG wavelengths are listed in Table 1. The macroscopic values of scattering efficiency (μ_{scat}), the absorption efficiency (μ_{abs}) and the anisotropy (g) for mouse skin tissue are taken from [26], and adapted for the two different wavelengths of the incident light and the SH emission.

Table 1. Tissue parameters used in the Monte-Carlo simulation.

Wavelength (nm)	Absorption cross-section μ_{abs} (cm^{-1})	Scattering cross-section μ_{scat} (cm^{-1})	Anisotropy g
812	0.15	260	0.95
406	3.2	580	0.8

In the model, we assume a narrow and highly directional beam reaching the tissue and we consider only the photons arriving within the area limited by the SHRIMP SHG cross-section. Moreover, we limit the angle of the photons reaching the SHRIMP ($\theta_{in} < 10°$) in order to take into account only photons that have undergone few scattering events, sometimes called snake photons [27]. After the first run of the Monte Carlo simulation, we obtain the local excitation intensity of a SHRIMP. We then calculate the SHG emission power from the SHRIMP according to the cross-section calculation (σ) of a 300 nm $BaTiO_3$ adapted from [16] for a 4π solid angle. A second Monte-Carlo simulation is then used for the SHG emission taking into account the numerical aperture of the objective. Thus we obtain the number of photons reaching the detector. We ran the simulation for different thicknesses of tissue as well as two different particle sizes (100 and 300 nm $BaTiO_3$).

Figure 6 displays the results of the simulations. The SHG signal decreases exponentially as a function of the tissue thickness, which is consistent with the previous reported studies [18]. The physical origin of this exponential decay is explained by the fact that the transmission coefficient in a medium with extinction (absorption or scattering) is an exponential function of the length of the medium. We calculate an extinction coefficient of 0.113 and 0.112 cm^{-1} for 100 and 300 nm SHRIMPs, respectively. In Fig. 6, we also show the approximate tissue thicknesses at which the 100 and 300 nm were still detectable at 50 and 120 μm, respectively. It is tempting to conclude from Fig. 6 that the minimum detectable signal level is several picowatts. Since the specification of the PMT sensitivity is only a few femtowatts, the noise floor is primarily determined by the background of endogenous SHG signal. It should be noticed that the simulation only considers the decrease in the signal strength due to the scattering by the tissue. It does not consider the endogenous SHG nor the detector noise which also contribute to the reduction in SNR with tissue thickness.

In order to obtain a complete theoretical estimate of the thickness at which we can detect SHRIMPs inside tissue we need to simulate the generation and subsequent scattering of the endogenous SHG signal as a function of tissue thickness. This is something we plan to do in the future; however, we believe that it may be possible to detect SHRIMPs at depths significantly larger than the 120 μm demonstrated here. There are several reasons for this. The detected power given in Fig. 6 is calculated from the experimental incident power, which is about 10 times below the cell damage threshold as mentioned earlier. Therefore, any increase of the incident power will improve the possible detectable depth of the SHRIMPs. Secondly, if the origin of the endogenous SHG signal is spatially separated from the location of the SHRIMP, then locally the SNR is very high. Finally, recently several techniques have been demonstrated that permit focusing through scattering media [1–3]. Eliminating or reducing the exponential loss of the signal decay through the scattering media (Fig. 6) would dramatically improve our ability to monitor SHRIMPs deep inside tissue.

#149795 - $15.00 USD Received 24 Jun 2011; revised 29 Jul 2011; accepted 29 Jul 2011; published 2 Aug 2011

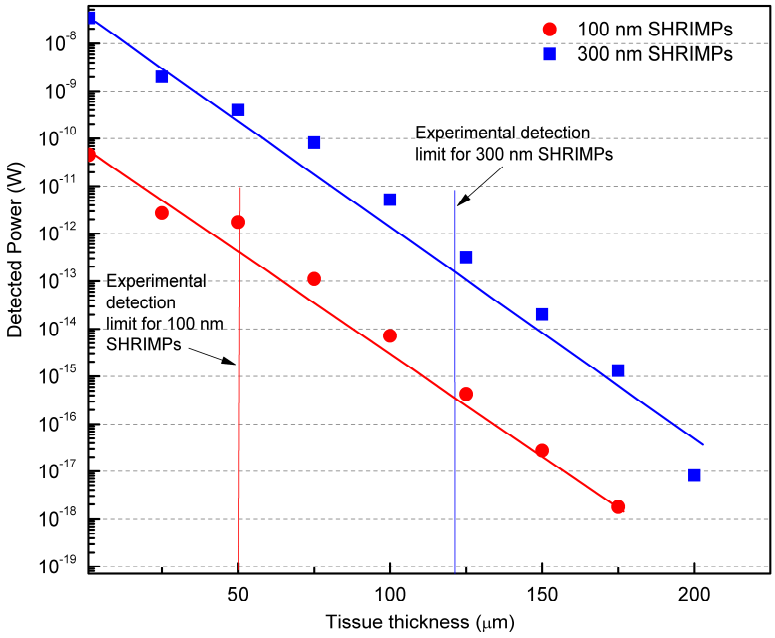

Fig. 6. Lin-log plot of the simulation results (data points) of the power detected from SHRIMP versus the thickness of the mouse tail tissue. Both simulated curves are fitted with a single exponential (solid lines). The red and blue vertical lines show the depth for which it is possible to experimentally detect 100 nm and 300 nm SHRIMP respectively.

5. Conclusion

We demonstrated that 100 and 300 nm $BaTiO_3$ nanoparticles can be efficiently used as second-harmonic radiation imaging probes in in vitro and in vivo tissues of mouse up to depth of 50 μm and 120 μm respectively. The contrast of the SHRIMPs is high enough to obtain a significant signal-to-noise ratio even with endogenous second-harmonic generation signals contributing to the background noise. Thus, the SHRIMPs can be used as flexible biomarkers in the same multiphoton microscope configuration as for two-photon fluorescence imaging, but they offer other functionalities such as no photobleaching or coherent signals that can be exploited in the future bioimaging applications.

Acknowledgments

The authors thank U. Haessler, M. Pasquier and W. Kilarski from M. Swartz's laboratory at EPFL for helping with the tissue and mice preparation performed by an accredited researcher under the authorization number 1954.3 delivered by the state of Vaud according to the Swiss legislation. We thank also M. Gyger for allowing the in vivo experiments, and T. Laroche from the BioImaging and Optics platform at EPFL for the imaging advices. The $BaTiO_3$ nanoparticles were kindly provided by Paul Bowen from EPFL and Vincenzo Buscaglia from the IENI in Genoa. This project is partly supported by the National Center of Competence in Research (NCCR), Quantum Photonics.